Electron affinity of gallium and fine structure of Ga^{−}: Experiment and theory

N. D. Gibson, C. W. Walter, C. Crocker, J. Wang, W. Nakayama, J. N. Yukich, Ephraim Eliav, and Uzi Kaldor

Phys. Rev. A **100**, 052512 — Published 26 November 2019

DOI: 10.1103/PhysRevA.100.052512

Electron Affinity of Gallium and Fine Structure of Ga^-: Experiment and Theory

N. D. Gibson, C. W. Walter*, C. Crocker†, J. Wang#, and W. Nakayama$
Department of Physics and Astronomy, Denison University, Granville, Ohio 43023, USA

J. N. Yukich
Physics Department, Davidson College, Davidson, North Carolina 28035, USA

Ephraim Eliav and Uzi Kaldor
School of Chemistry, Tel Aviv University, 69978 Tel Aviv, Israel

ABSTRACT

Binding energies of fine structure levels of the negative ion of gallium have been determined both experimentally and theoretically, resolving long-standing discrepancies for the electron affinity of gallium. The relative photodetachment cross section from Ga^- ($4p^2\ ^3P_{0,1,2}$) was measured using tunable laser spectroscopy over the photon energy range 270 – 400 meV (4600 - 3100 nm). Observed photodetachment thresholds were used to measure the electron affinity of Ga to be 301.20(11) meV and the fine structure splittings of Ga^- to be 23.31(19) meV for $J = 0–1$ and 62.4(5) meV for $J = 0–2$. The binding energies of the negative ion states were independently calculated using the multireference extrapolated intermediate Hamiltonian relativistic Fock-space coupled cluster method in large, converged four-component Gaussian-spinor basis sets. The Dirac-Fock-Breit Hamiltonian was used, and leading quantum electrodynamic effects were added. All calculations were carried out in spherical symmetry, correlating all electrons and fully including core effects. The calculated electron affinity is 302(3) meV, and the fine structure splittings are 22(2) meV for $J = 0–1$ and 60(2) meV for $J = 0–2$, which are all in excellent agreement with the present measurements. These results substantially improve both the accuracy and precision of the Ga electron affinity and provide the first determination of the fine structure of Ga^-.

*Electronic address: walter@denison.edu.

[†]Present address: Keysight Technologies, 1400 Fountaingrove Parkway, Santa Rosa, CA 95403, USA.

[#]Present address: Department of Physics and Astronomy, University of Nebraska-Lincoln, Lincoln, NE 68588, USA.

[$]Present address: Department of Electrical and Systems Engineering, University of Pennsylvania, Philadelphia, PA 19104, USA.

I. Introduction

Negative ions are of interest for both applied and fundamental reasons [1]. Electron correlation usually plays an important role in determining the stability of negative ions. The binding energy of a negative ion (corresponding to the electron affinity of the neutral) is extremely sensitive to multi-electron interactions, thus negative ions serve as important tests of detailed atomic structure calculations and yield key insights into dynamical correlation effects.

Through substantial research efforts over the past three decades, the electron affinities (EAs) of most elements have now been well-established with measured precisions in the sub-meV range and agreement between theory and experiment at the few meV level [2-4]. However, the EAs of the Group 13 elements (B, Al, Ga, In, and Tl) have been particularly challenging to pin down in part because their negative ions are weakly bound [2,3], and up to now significant discrepancies remain for gallium and thallium [4]. For Ga, the best previously available experimental value for the EA differs by more than 100 meV from most theoretical calculations [2,4]. The present study resolves this discrepancy for Ga through both high-precision experimental and theoretical investigations of its negative ion Ga^-.

The ground state valence configuration of neutral Ga is $4p\ ^2P_{1/2}$, and the configuration of the bound negative ion Ga^- is $4p^2\ ^3P_{0,1,2}$ with the lowest energy level being $J = 0$ (see the energy level diagram in Fig. 1). The first detailed experimental investigation of Ga^- was performed by Williams *et al.* [5] using fixed-frequency laser photodetachment electron spectroscopy yielding 430(30) meV for the electron affinity of Ga. A subsequent reanalysis of the data of Williams *et al.* by Hotop including estimated fine structure effects gave an electron affinity of 410(40) meV [6].

A large number of theoretical studies of the electron affinity of Ga have been reported using a variety of calculational methods [4,7-14]. The calculated EAs range from 222 - 318

meV, with most values clustering near 300 meV (see Table II for a summary of theoretical results). All of the theoretical calculations give electron affinities that are substantially lower than the previous experimental value by ~100 meV or more. These substantial discrepancies between theoretical and experimental values highlight the need for further detailed investigation.

In the present study, photodetachment threshold spectroscopy with a tunable mid-infrared laser was used to measure the electron affinity of Ga and the fine structure energy splittings of Ga^- with sub-meV precision. In addition to the experiments, independent theoretical calculations of the bound states of Ga^- were performed using the multireference extrapolated intermediate Hamiltonian relativistic Fock-space coupled cluster method with large-scale basis sets and comprehensive inclusion of correlation, Breit, and quantum electrodynamic (QED) effects. The calculations are in excellent agreement with the experimental binding energies to the meV level. The present results substantially improve the precision of the Ga electron affinity, resolve the previous discrepancies, and provide the first determination of the fine structure of Ga^-.

II. Experimental Method and Measured Spectrum

In the present experiments, photodetachment from Ga^- was measured as a function of photon energy using a crossed ion-beam—laser-beam system that has been described in detail previously [15,16]. Negative ions were produced by a cesium sputter ion source (NEC SNICS II) [17] using a cathode packed with Ga_2O_3 powder. The ions were accelerated to 12 keV and the $^{69}Ga^-$ isotope was magnetically mass selected; typical currents of Ga^- were ~100 pA. In the interaction region, the ion beam was intersected perpendicularly by a pulsed laser beam. Following the interaction region, residual negative ions were electrostatically deflected into a Faraday cup, while neutral atoms produced by photodetachment continued undeflected to a

multi-dynode particle multiplier detector. The neutral atom signal was normalized to the ion-beam current and the laser photon flux measured for each laser pulse. The spectra were obtained by repeatedly scanning the laser wavelength continuously over a range and then sorting the data into photon energy bins of selectable width, as previously described by Walter *et al.* [15].

The laser system consisted of a tunable optical parametric oscillator-amplifier (OPO-OPA) (LaserVision) pumped by a pulsed Nd:YAG laser. The mid-infrared "idler" output of the OPA was used in the present measurements, giving an operating range of 250 – 585 meV (5000 – 2120 nm) with a bandwidth of ~0.07 meV. The wavelength of the mid-infrared light was determined for each laser pulse using a procedure fully described in [15]; briefly, a pulsed wave meter (High Finesse WS6–600) measured the wavelength of the OPO "signal" light, which was then used with the measured pump laser wavelength to determine the wavelength of the OPA "idler" light by conservation of energy. The laser beam diverges slightly as it leaves the OPA, so a long focal length lens (~2 m focal length) was placed in the beam path ~2 m from the interaction region to approximately collimate the beam. In the interaction region, the laser pulse had a typical energy of ~50 μJ, pulse duration of ~5 ns, and beamwidth of ~0.25 cm. To reduce room air absorption by strong H_2O and CO_2 bands in the mid-infrared [18], a tube flushed with dry nitrogen gas was used to enclose the laser beam path from the OPA to the vacuum chamber entrance window. The photon energy calibration in the mid-infrared was verified by measuring several sharp absorption dips due to ambient H_2O vapor; the measured energies agreed with tabulated values from the HITRAN database [18] to within the uncertainty of ~0.01 meV.

The relative photodetachment cross section from Ga^- measured over the photon energy range 275 – 350 meV is shown in Fig. 2. This spectrum shows three nested thresholds due to photodetachment from different fine structure levels of Ga^- to different fine structure levels of Ga. As fully explained below, these three thresholds can be definitively identified in increasing

energy order as $^3P_1 \rightarrow {}^2P_{1/2}$, $^3P_0 \rightarrow {}^2P_{1/2}$, and $^3P_2 \rightarrow {}^2P_{3/2}$. The background signal below the $^3P_1 \rightarrow {}^2P_{1/2}$ threshold is due to photodetachment from $^3P_2$ at lower photon energies; it was not possible to operate the OPO-OPA at photon energies low enough to reach the threshold for $^3P_2 \rightarrow {}^2P_{1/2}$ detachment near 239 meV. In addition to the three thresholds shown in Fig. 2, a weak threshold was observed at higher energies near 380.5 meV for $^3P_1 \rightarrow {}^2P_{3/2}$ detachment. It was not possible, however, to distinguish the $^3P_0 \rightarrow {}^2P_{3/2}$ threshold at even higher energies, because of the weakness of this channel and the large background signal due to detachment from all of the lower energy channels.

The identification of the observed thresholds and determination of their energies is facilitated by fitting the measured photodetachment spectrum with standard functions. For a limited range above an opening threshold, the photodetachment cross section is characterized by the Wigner threshold law [19]:

$$\sigma = \sigma_0 + a \cdot (E - E_t)^{\ell + 1/2} \qquad (1)$$

where E is the photon energy, E_t is the threshold energy, ℓ is the orbital angular momentum of the departing electron, and a is the relative strength coefficient. The background cross section due to photodetachment to lower energy thresholds is represented by σ_0, which may be energy dependent. In the present experiments, a p electron is detached from the Ga^- ion. Thus, the angular momentum selection rule $\Delta\ell = \pm 1$ dictates that the departing electron will be either s or d; near threshold, the s-wave contribution ($\ell = 0$) dominates the total cross section.

As the energy above threshold increases, the photodetachment cross section progressively deviates from the Wigner law due to long-range interactions between the departing electron and the remaining neutral atom, such as polarization forces [20]. Farley [21] derived an expression for the leading term correction to the Wigner law based on the zero-core-contribution model of

photodetachment [22], which for detachment of a *p* electron gives the following modified *s*-wave Wigner law with leading correction:

$$\sigma = \sigma_0 + a \cdot [(E - E_t)^{1/2} + b \cdot (E - E_t)^{3/2}] \qquad (2)$$

The additional correction term depending on energy above threshold to the 3/2 power has a negative coefficient *b*, causing progressively larger reductions in the cross section relative to the pure *s*-wave Wigner law as the energy increases.

Figure 2 shows a fit of the *s*-wave Wigner law with leading correction (Eq. (2)) to the measured photodetachment spectrum with three thresholds included. In this fit, the threshold energies E_t and relative strengths *a* were allowed to be adjusted separately for each threshold, but the coefficient of the correction term *b* was kept at the same value for all three thresholds. The *s*-wave Wigner law with leading correction provides an excellent representation of the data throughout the measured range of tens of meV above the individual thresholds. The measured relative strengths *a* of the three photodetachment channels derived from the fit of Eq. (2) to the spectrum in Fig. 2 are given in Table I.

To identify the observed thresholds, the measured channel strengths can be compared to estimated strengths obtained from general theoretical considerations. The fine structure transition intensities for one-electron detachment from a generic *L*-*S* coupled negative ion can be calculated using the model developed by Engelking and Lineberger based on evaluation of the reduced transition matrix elements and Clebsch-Gordon coefficients [23]. This calculated transition intensity is then weighted by the population distribution of the initial ion fine structure levels to obtain an estimate of the relative channel strengths. For the weighting of initial ion levels in the present case, we used a thermal Boltzmann distribution at a temperature of 1600 K, which is the approximate temperature of the ionizer in the ion source for the present experiments.

The estimated channel strengths obtained in this way for the six possible fine structure transitions from Ga^- ($^3P_{0,1,2}$) to Ga ($^2P_{1/2,3/2}$) are shown in Table I.

In comparing the measured and estimated channel strengths for the different fine structure transitions (see Table I), it is readily apparent that the only matching assignment is to identify the three thresholds in the spectrum of Fig. 2 in increasing energy order as $^3P_1 \rightarrow {}^2P_{1/2}$, $^3P_0 \rightarrow {}^2P_{1/2}$, and $^3P_2 \rightarrow {}^2P_{3/2}$. With this identification, the measured strengths of the three channels (2.3(3), 1, and 5.1(6), respectively) are in quite reasonable agreement with the corresponding estimated strengths (1.9, 1, and 4.0, respectively). Conversely, the alternative options of identifying the lowest energy threshold as either $^3P_2 \rightarrow {}^2P_{1/2}$ or $^3P_0 \rightarrow {}^2P_{1/2}$, i.e. shifting the measured results in Table I either one row higher or one row lower, would lead to complete disagreement between the measured and estimated strengths. It is also worth noting that the moderate differences between the measured and estimated strengths for the assigned transitions in Table I are not surprising due to the limitations of the L-S model, the lack of specific information about the effective temperature of the ion source (a higher assumed temperature would lead to closer agreement), and possible deviation of the initial fine structure population distribution from thermal due to the energetic sputtering process. Thus, the relative channel strengths give unambiguous evidence for the threshold assignments shown in Table I; further strong support for the assignments comes from the excellent agreement between the present experimental and theoretically calculated Ga electron affinity and Ga^- fine structure splittings, as discussed in Sec. IV.

In order to accurately determine the threshold energies, narrow scans were taken near the thresholds to improve the signal-to-noise ratios. A scan near the Ga^- ($4p^2\ ^3P_0$) → Ga ($4p\ ^2P_{1/2}$) ground-state to ground-state threshold, which defines the electron affinity, is shown in Fig. 3. A fit of the *s*-wave Wigner law (Eq. (1)) including a linear background term gives excellent

agreement with the data in this narrow range near threshold. To assess the range of validity of the Wigner law and the effects of possible background changes, photodetachment cross section measurements were taken over somewhat larger photon energy ranges near threshold (~ ±6 meV), and the low and high energy ends were successively trimmed to narrow the range of the fit and determine the most accurate threshold value. Deviations from the Wigner law were found as little as ~3 meV above threshold for the transitions in the present study. In addition, fits were performed with the background held constant for small ranges near threshold, rather than the linear background, and the fitted threshold values were the same within uncertainties. The data were also analyzed using a range of photon energy bin widths from 0.3 to 5 times the laser bandwidth, and the fitted threshold values were found to be independent of the chosen bin width within uncertainties. Fits were also performed with the *s*-wave Wigner law with the leading correction function (Eq. (2)) over wider photon energy ranges, which gave thresholds that agreed within uncertainties with those derived from the narrow scans fit with the pure *s*-wave Wigner law.

The measured threshold energies for the observed transitions are presented in Table I. Multiple measurements were taken of each threshold, and the weighted averages were used to determine the final values. The quoted one-sigma uncertainties include statistical uncertainties associated with the fits (the major contributor to the overall uncertainty), photon energy calibration and bandwidth uncertainties, and potential Doppler shifts due to possible deviation of the ion – laser beam intersection angle from perpendicular. Another consideration when using pulsed lasers, especially in the mid-infrared, is that the ponderomotive effect can shift the photodetachment threshold [24]. However, in the present experiments, the laser was not strongly focused as discussed earlier, so the peak intensity in the interaction region was only ~5×10^4 W/cm^2, which gives a negligibly small ponderomotive threshold shift of only ~1×10^{-4} meV.

The measured EA of Ga determined from the $^3P_0 \rightarrow {}^2P_{1/2}$ threshold is 301.20(11) meV. The Ga^- $J = 0–1$ fine structure splitting is determined by subtracting the measured threshold for $^3P_1 \rightarrow {}^2P_{1/2}$ from the threshold for $^3P_0 \rightarrow {}^2P_{1/2}$. The Ga^- $J = 0–2$ fine structure splitting is determined by subtracting the threshold for $^3P_2 \rightarrow {}^2P_{3/2}$ from the sum of the threshold for $^3P_0 \rightarrow {}^2P_{1/2}$ plus the well-known Ga $J = 1/2–3/2$ splitting energy of 102.4345 meV [25]. The fine structure splittings of Ga^- are measured to be 23.31(19) meV for $J = 0–1$ and 62.4(5) meV for $J = 0–2$ (and 39.1(5) meV for $J = 1–2$). The Ga^- $J = 0–1$ splitting was further confirmed by the observed $^3P_1 \rightarrow {}^2P_{3/2}$ threshold, which gives a splitting of 23.1(13) meV for $J = 0–1$ in agreement with the more precise value from the lower threshold. Tables II and III summarize the present results for the EA of Ga and the fine structure splittings of Ga^-.

III. Theoretical Calculations

The relativistic multireference Fock-space coupled cluster method and its numerous applications to heavy and superheavy elements have been described in several recent reviews [26-28]. Excellent agreement with measurements has been demonstrated, so that reliable prediction of unknown properties can be made. We quote just two examples: (i) The ionization potential of lawrencium was calculated at 4.963(15) eV and the experiment yielded 4.96(8) eV [29]; (ii) The ionization potential of astatine was predicted at 9.307(25) eV and measured as 9.31751(8) eV [30]. In both cases, the calculations were completed before experimental values became available. These two examples employed the single-reference CCSD(T) scheme; here we preferred to use the multireference approach of the intermediate Hamiltonian Fock-space coupled cluster (IHFSCC) method, which gave meV agreement with experimental EAs for all

alkali atoms [31]. The Ga^- negative ion has two electrons outside closed shells, similar to the alkali negative ions.

Here we start from the closed-shell Ga^+ positive ion, adding one or two electrons to obtain the relevant states of the Ga atom and its negative ion. The basis set is increased systematically to convergence of the calculated energies. Likewise, systematic extension of the size of the model space P by the extrapolated intermediate Hamiltonian (XIH) extension of the Fock-space coupled cluster (FSCC) method [32] makes possible the inclusion of correlation effects well beyond the coupled cluster single double (CCSD) approximation.

Our methods and programs use spherical coordinates. In that they differ fundamentally from the methods available in the DIRAC package [33] used recently by Finney and Peterson [4], which works in Cartesian coordinates. This limits us to atoms only, whereas DIRAC can handle molecules. On the plus side, we can use much larger basis sets: adding an ℓ orbital means 2 more functions in spherical coordinates vs. $2\ell+1$ functions in Cartesian, so we can go to high ℓ and achieve convergence without resorting to corrections or extrapolations. All electrons are correlated explicitly, and all significant terms in the Hamiltonian are treated simultaneously. It may be more convenient computationally to add up a number of contributions calculated separately (see [4]), but various contributions may not always be additive. A well-known example is the non-additivity of relativistic and correlation effects in heavy elements, associated with the strong relativistic contraction of s and $p_{1/2}$ orbitals, which in turn increases their correlation effects. The importance of treating relativity and correlation together is demonstrated by the determination of the ground state of rutherfordium, Rf [34]. The atom has two low-lying electron configurations, with $6d^27s^2$ or $6d7s^27p$ electrons outside the $[Rn]5f^{14}$ closed shells. Studies showed [34] that including correlation more exactly favors the second state, whereas better representation of relativity favors the first. The two effects had to be treated together to

high order, indicating unequivocally that the ground state of Rf is $6d^2 7s^2$. The relatively light Ga should not be subject to these problems, but care must be taken when handling heavier elements.

We use the Dirac-Coulomb-Breit Hamiltonian (DCBH), which includes all terms up to second order in the fine-structure constant α. The leading QED terms are included by adding the Shabaev *et al.* Lamb shift model potential [35] to the DCBH. Electron correlation is treated by the Fock-space coupled cluster method and its intermediate Hamiltonian extension [26-28]. The basis set is increased systematically until results converge. In the present case we used two different families of basis sets, the universal set [36], with exponents forming a geometric progression, and the Huzinaga set [37]. Each set was extended by adding functions to convergence. The converged Huzinaga basis went up to ℓ = 8, consisting of 35*s*30*p*25*d*20*f*11*g*9*h*9*i*7*j*7*k* functions, and the converged universal set included 37*s*32*p*24*d*21*f*12*g*10*h*9*i*7*j*7*k* functions. The model spaces used for the electron attachment calculations were obtained by adding orbitals until the levels of the negative ion converged. The valence active space was constructed from all suitable combinations of the 6*s*-10*s*, 4*p*-9*p*, 5*d*-8*d* and 4*f*-6*f* orbitals, giving over 6000 determinants for each of the two basis sets. The two converged sets gave very close results, agreeing to better than 0.5 meV for the EA and 0.2 meV for the fine structure splittings. This gives an estimate of the error limit associated with the basis. The final value for the lowest electron affinity of Ga, giving the $4p^2\ ^3P_0$ state, was 302 meV. The fine structure energies going to the higher $^3P_1$ and $^3P_2$ states were 22 meV and 60 meV, respectively. The possible contribution of higher-order correlation was estimated by applying the extrapolated intermediate Hamiltonian scheme (XIH-FSCC) [32]; the change from the FSCC results was 1 meV for the EA and 0.7 meV for the fine structure splittings. The final source of error is due to high-order relativistic effects; these were estimated to be less than 50% of the calculated Breit interaction and Lamb shift, 1 meV for the EA and 0.7 meV for the fine structure

splittings. Our final calculated values are therefore 302(3) meV for the EA, 22(2) meV for $J = 0–1$, and 60(2) meV for $J = 0–2$.

Our calculated values agreed with the present experiment at the meV level. We were therefore surprised by the recent results of Finney and Peterson [4], which showed a much smaller EA, 5.25 kcal/mol or 228 meV. Looking at the data in their Table IV, we found that they used an incorrect value for the spin-orbit contribution ΔSO. This term was obtained from their Table III as the sum of the Gaunt and KRCI terms, listed as +0.01 kcal/mol and -0.50 kcal/mol respectively. Unfortunately, the sum appeared in Table IV as -2.21 kcal/mol rather than -0.49 kcal/mol, giving an erroneous EA. Using the correct ΔSO value, we found that the EA from Finney and Peterson's calculation comes out as 6.97 kcal/mol or 302 meV [38,39], closely matching the experimental and computed values obtained in the present work. Thus, the EA of Ga has now been confirmed by three separate approaches.

IV. Results and Discussion

The results for the electron affinity of Ga are listed together with previous results in Table II. The present calculated EA of 302(3) meV is in excellent agreement with the present measured value of 301.20(11) meV, well within the uncertainty range. We stress that the calculations were completed independently from the experiments.

The present measured EA of 301.20(11) meV is significantly different from the previous measurement of 430(30) meV by Williams *et al.* [5]. Williams *et al.* used the technique of laser photodetachment electron spectroscopy (LPES), in which the kinetic energies of the ejected electrons were measured following photodetachment with a fixed frequency laser. This technique is very good for obtaining exploratory information about a negative ion; however, calibration of the absolute kinetic energy scale for the photoelectrons is a substantial challenge

[1-3]. Limited resolution can be another challenge for LPES, and in the experiment by Williams *et al.* it was not possible to resolve the fine structure contributions due to either the negative ion or neutral atom. Subsequently, Hotop reanalyzed the data of Williams *et al.* including estimated fine structure effects, obtaining a revised value of the Ga electron affinity of 410(40) meV [6]. While this revised value does bring the previous electron affinity slightly closer to the current value, the remaining substantial difference suggests that the earlier LPES measurement may have been affected by additional factors such as non-thermal fine structure channel strengths or energy calibration issues. In contrast to the limitations of LPES, the laser photodetachment threshold spectroscopy technique used in the present study gives much higher resolution to separate the fine structures, as well as greater precision since it relies on the straightforward measurement of laser wavelengths to set the energy scale. Furthermore, the high precision of threshold spectroscopy used in the present experiment permitted a reduction in the uncertainties from the previous measurements for the electron affinity of Ga by a factor of ~300, from 30 - 40 meV to only 0.11 meV.

Most of the numerous previous theoretical calculations of the EA of Ga are in good agreement with the present value at the 10 - 20 meV level, and several are within 4 meV (see Table II). In contrast, a much smaller EA was obtained by Felfli *et al.* using the Regge pole method [14]; this method is a very different approach from the other calculational techniques, and it is not readily apparent what causes the difference for that value. It should also be noted that the detailed large-scale calculations performed in the present study yielded significantly higher precision than previous theoretical studies, reducing the estimated uncertainty in the calculated EA to only 3 meV.

The present results for the fine structure splittings of Ga^- are presented in Table III. As for the EA, the calculated values are in excellent agreement with the measured values within uncertainties. Table III also lists the estimated fine structure splittings based on isoelectronic extrapolation [40,41]; the estimated values are in fair agreement with the present precise measurements, considering the substantial uncertainties involved in the extrapolation method.

Our interpretation of the measured photodetachment spectrum, and thus our experimental determination of the electron affinity of Ga, is strongly supported by several factors. The measured relative strengths of the detachment channels are consistent with the estimated channel strengths of the different fine structure transitions, giving confidence in our identifications of the observed photodetachment thresholds. Furthermore, we were able to observe detachment thresholds from Ga^- $^3P_1$ to both Ga $^2P_{1/2}$ and $^2P_{3/2}$; the separation of these two measured thresholds matches the accepted Ga $J = 1/2–3/2$ splitting [25]. Finally, there is excellent agreement between the present measured and theoretically calculated values for both the electron affinity of Ga and the fine structure splittings of Ga^-, clearly resolving the long-standing discrepancies between previous studies.

V. Conclusions

In summary, we have used photodetachment threshold spectroscopy to determine the electron affinity of Ga to be 301.20(11) meV. The present measurement significantly revises the experimental value of the EA of Ga and reduces its uncertainty by a factor of ~300. In addition, the fine structure of Ga^- has been measured for the first time. The experimental measurements are further supported by independent large-scale theoretical calculations, which yield values for the binding energies of Ga^- in complete agreement with the experiments. The present results

resolve the long-standing discrepancies for the negative ion of gallium and provide precise information that can serve as a test for evaluating theoretical approaches to atomic structure calculations involving multi-electron interactions and correlation effects.

Overall for Group 13 elements, there now appears to be good agreement between the experimental electron affinities and most theoretical calculations for all members except the heaviest atom of the group, thallium. Significant discrepancies remain between the measured value for the electron affinity of Tl (377(13) meV [42]) and many of the calculated theoretical values [2-4]. We have recently performed a similar experimental study of Tl^- using infrared photodetachment threshold spectroscopy to precisely measure the binding energy of the negative ion and help resolve the previous discrepancies [43]; these results will be fully reported in the future.

ACKNOWLEDGMENTS

We thank Dave Burdick, Archie Jugdersuren, and Rob Ficken for technical assistance. This material is based in part upon work supported by the National Science Foundation under Grant Nos. 1068308, 1404109, and 1707743. WN received partial support from Denison University's Anderson Summer Research Fund.

REFERENCES

[1] D. J. Pegg, Rep. Prog. Phys. **67**, 857 (2004).

[2] T. Andersen, H. K. Haugen, and H. Hotop, J. Phys. Chem. Ref. Data **28**, 1511 (1999).

[3] T. Andersen, Phys. Rep. **394**, 157 (2004).

[4] B. A. Finney and K. A. Peterson, J. Chem. Phys. **151**, 024303 (2019).

[5] W. W. Williams, D. L. Carpenter, A. M. Covington, M. C. Koepnick, D. Calabrese, and J. S. Thompson, J. Phys. B **31**, L341 (1998).

[6] H. Hotop (unpublished, 1998), cited in Ref. 2.

[7] F. Arnau, F. Mota, and J. J. Novoa, Chem. Phys. **166**, 77 (1992).

[8] E. Eliav, Y. Ishikawa, P. Pyykkö, and U. Kaldor, Phys. Rev. A **56**, 4532 (1997).

[9] W. P. Wijesundera, Phys. Rev. A **55**, 1785 (1997).

[10] D. Sundholm, M. Tokman, P. Pyykkö, E. Eliav, and U. Kaldor, J. Phys. B **32**, 5853 (1999).

[11] C. Guo-Xin and P. P. Ong, Journal of Physics B: Atomic, Molecular and Optical Physics **32**, 5351 (1999).

[12] D. Figgen, A. Wedig, H. Stoll, M. Dolg, E. Eliav, and U. Kaldor, J. Chem. Phys. **128**, 024106 (2008).

[13] J. Li, Z. Zhao, M. Andersson, X. Zhang, and C. Chen, J. Phys. B-At. Mol. Opt. Phys. **45**, 165004 (2012).

[14] Z. Felfli, A. Z. Msezane, and D. Sokolovski, J. Phys. B-At. Mol. Opt. Phys. **45**, 189501 (2012).

[15] C. W. Walter, N. D. Gibson, D. J. Carman, Y.-G. Li, and D. J. Matyas, Phys. Rev. A **82**, 032507 (2010).

[16] C. W. Walter, N. D. Gibson, Y.-G. Li, D. J. Matyas, R. M. Alton, S. E. Lou, R. L. Field III, D. Hanstorp, L. Pan, and D. R. Beck, Phys. Rev. A **84**, 032514 (2011).

[17] R. Middleton, *A Negative-Ion Cookbook* (Dept. of Physics, Philadelphia, PA, 1990).

[18] L. S. Rothman, I. E. Gordon, A. Barbe, *et al.*, J. Quant. Spect. Rad. Tran. **110**, 533 (2009).

[19] E. P. Wigner, Phys. Rev. **73**, 1002 (1948).

[20] T. F. O'Malley, Phys. Rev. **137**, A1668 (1965).

[21] J. W. Farley, Phys. Rev. A **40**, 6286 (1989).

[22] R. M. Stehman and S. B. Woo, Phys. Rev. A **20**, 281 (1979).

[23] P. C. Engelking and W. C. Lineberger, Phys. Rev. A **19**, 149 (1979).

[24] M. D. Davidson, J. Wals, H. G. Muller, and H. B. van Linden van den Heuvell, Phys. Rev. Lett. **71**, 2192 (1993)

[25] A. Kramida, Yu. Ralchenko, J. Reader, and NIST ASD Team (2018). *NIST Atomic Spectra Database* (ver. 5.6.1), [Online]. Available: https://physics.nist.gov/asd [2019, August 24]. National Institute of Standards and Technology, Gaithersburg, MD.

[26] E. Eliav, A. Borschevsky, and U. Kaldor, *Handbook of Relativistic Quantum Chemistry*, Edited by W. Liu (Springer Berlin, Heidelberg, 2016), p. 825.

[27] E. Eliav and U. Kaldor, *Relativistic Methods for Chemists*, Edited by M. Barysz and Y. Ishikawa (Springer, Netherlands, 2010), p. 279.

[28] E. Eliav and U. Kaldor, *Recent Progress in Coupled Cluster Methods: Theory and Applications*, Edited by J. Pittner, P. Charsky and J. Paldus (Springer, Heidelberg, 2010), p. 113.

[29] T. K. Sato, M. Asai, A. Borschevsky*, et al.*, Nature **520**, 209 (2015).

[30] S. Rothe, A. N. Andreyev, S. Antalic*, et al.*, Nature Communications **4**, 1835 (2013).

[31] A. Landau, E. Eliav, Y. Ishikawa, and U. Kaldor, J. Chem. Phys. **115**, 2389 (2001).

[32] E. Eliav, M. J. Vilkas, Y. Ishikawa, and U. Kaldor, J. Chem. Phys. **122**, 224113 (2005).

[33] DIRAC, a relativistic ab initio electronic structure program, release DIRAC16 (2016), written by H. J. Aa. Jensen, R. Bast, T. Saue, and L. Visscher, with contributions from V. Bakken, K. G. Dyall, S. Dubillard, U. Ekstroem, E. Eliav, T. Enevoldsen, E. Fasshauer, T. Fleig, O. Fossgaard, A. S. P. Gomes, T. Helgaker, J. Henriksson, M. Ilias, Ch. R. Jacob, S. Knecht, S. Komorovsky, O. Kullie, J. K. Laerdahl, C. V. Larsen, Y. S. Lee, H. S. Nataraj, M. K. Nayak, P. Norman, G. Olejniczak, J. Olsen, Y. C. Park, J. K. Pedersen, M. Pernpointner, R. Di Remigio, K. Ruud, P. Salek, B. Schimmelpfennig, J. Sikkema, A. J. Thorvaldsen, J. Thyssen, J. van Stralen, S. Villaume, O. Visser, T. Winther, and S. Yamamoto, see http://www.diracprogram.org .

[34] E. Eliav, U. Kaldor, and Y. Ishikawa, Phys. Rev. Lett. **74**, 1079 (1995).

[35] V. M. Shabaev, I. I. Tupitsyn, V. A. Yerokhin, Phys. Rev. A **88**, 012513 (2013).

[36] G. L. Malli, A. B. F. Da Silva, and Y. Ishikawa, Phys. Rev. A **47**, 143 (1993).

[37] S. Huzinaga and M. Klobukowski, Chem. Phys. Lett. **212**, 260 (1993).

[38] This corrected value for the EA of [4] was subsequently confirmed by the authors of [4], K. A. Peterson (private communication).

[39] A similar error in the ΔSO term also appeared in [4] for the calculated EA of In. The corrected calculated EA of In using the correct ΔSO term is 8.91 kcal/mol rather than 7.69 kcal/mol, which is very close to the experimental value of 8.8534(14) kcal/mol from Walter *et al.* [15].

[40] R. J. Zollweg, J. Chem. Phys. **50**, 4251 (1969).

[41] H. Hotop and W. C. Lineberger, J. Phys. Chem. Ref. Data **4**, 539 (1975).

[42] D. L. Carpenter, A. M. Covington, and J. S. Thompson, Phys. Rev. A **61**, 042501 (2000).

[43] C. W. Walter, N. D. Gibson, K. R. Patel, and S. E. Spielman, in *APS-DAMOP Meeting Abstracts (*Milwaukee, Wisconsin, USA, May, 2019), p. E01.00004.

TABLE I. Measured threshold energies and measured and calculated relative channel strengths for Ga^- (^3P_J) → Ga ($^2P_{J'}$) transitions. The measured threshold energies are obtained from fits of the *s*-wave Wigner law (Eq. (1)) to the measured relative photodetachment cross section over narrow ranges near the four thresholds observed in the present experiments. The measured relative strengths are obtained from a fit of the *s*-wave Wigner law with leading correction (Eq. (2)) to the measured photodetachment spectrum of Fig. 2 with three thresholds included. The estimated relative strengths are obtained from the calculated *L-S* model fine structure transition intensities [23] weighted by a thermal initial ion level distribution at 1600 K, as discussed in the text.

Transition	**Measured Threshold Energy E_t (meV)**	**Relative Strength**	
		Measured	**Estimated**
$^3P_2 \rightarrow {}^2P_{1/2}$	--	--	0.8
$^3P_1 \rightarrow {}^2P_{1/2}$	277.89(16)	2.3(3)	1.9
$^3P_0 \rightarrow {}^2P_{1/2}$	301.20(11)	1.0	1.0
$^3P_2 \rightarrow {}^2P_{3/2}$	341.3(5)	5.1(6)	4.0
$^3P_1 \rightarrow {}^2P_{3/2}$	380.5(13)	--	1.9
$^3P_0 \rightarrow {}^2P_{3/2}$	--	--	0.5

TABLE II. Comparison of the present results for the electron affinity of Ga to previous measurements and theoretical calculations. Methods - Experiment: LPTS = Laser photodetachment threshold spectroscopy, LPES = Laser photodetachment electron spectroscopy; Theory: XIH-RFSCC = Extrapolated intermediate Hamiltonian extension of the relativistic Fock-space coupled cluster, CIPSI = Multireference configuration interaction, MCDF = Multiconfiguration Dirac-Fock, RFSCC = Relativistic Fock-space coupled cluster, MCHF-CCSD = Multiconfiguration Hartree-Fock with coupled cluster, IHFSCC = Intermediate-Hamiltonian Fock-space coupled cluster, MCDHF = Multiconfiguration Dirac-Hartree-Fock, RCC-FPD = Relativistic coupled-cluster version of the Feller-Peterson-Dixon composite method.

Study	**Method**	**Electron Affinity (meV)**
Experiment		
Present experiment	LPTS	301.20(11)
Williams *et al.* [5]	LPES	430(30)
Hotop [6]	Reanalysis of Ref. [5]	410(40)
Theory		
Present theory	XIH-RFSCC	302(3)
Arnau *et al.* [7]	CIPSI	290
Eliav *et al.* [8]	RFSCC	305
Wijesundera [9]	MCDF	301
Sundholm *et al.* [10]	MCHF-CCSD	297(13)
Guo-Xin & Ong [11]	RHF-DFT	318
Figgen *et al.* [12]	IHFSCC	298
Li *et al.* [13]	MCDHF	317.97
Felfli *et al.* [14]	Regge pole	222
Finney and Peterson [4]	RCC-FPD	228(22)
Corrected EA of Ref. [4]	[a]	302(22)[a]

[a] Corrected electron affinity of [4] using the correct ΔSO value, as discussed in the text [38].

TABLE III. Fine structure splittings for the bound states of Ga^- ($^3P_{0,1,2}$) determined in the present study and estimated by isoelectronic extrapolation [40,41].

Study	$J = 0 - 1$ **(meV)**	$J = 0 - 2$ **(meV)**
Present Experiment	23.31(19)	62.4(5)
Present Theory	22(2)	60(2)
Isoelectronic Extrapolation [40,41]	27.3(2.5)	72(6)

FIGURE CAPTIONS

FIG. 1. (color online) Energy level diagram for the fine structure levels of the $4p^2\ ^3P$ state of Ga^- and the $4p\ ^2P$ state of Ga. The energies of the Ga^- states are based on the present measurements and the energy of the Ga J=3/2 state is from [25]. The thresholds measured in the present study are shown by vertical arrows, with the electron affinity defining threshold shown in bold red.

FIG. 2. (color online) Measured photodetachment spectrum from Ga^- showing the three lowest energy thresholds observed in the present study. The data points (circles) include 1-sigma statistical error bars. The solid line is a fit to the data of three nested *s*-wave Wigner law with the leading correction functions (Eq.(2)).

FIG. 3. (color online) A fit of the *s*-wave Wigner law (Eq. (1)) (solid line) to the measured relative photodetachment cross-section data (circles) near the threshold for the Ga^- ($^3P_0$) to Ga ($^2P_{1/2}$) ground-state-to-ground-state transition. The energy of this threshold corresponds to the electron affinity of Ga.

FIGURE 1

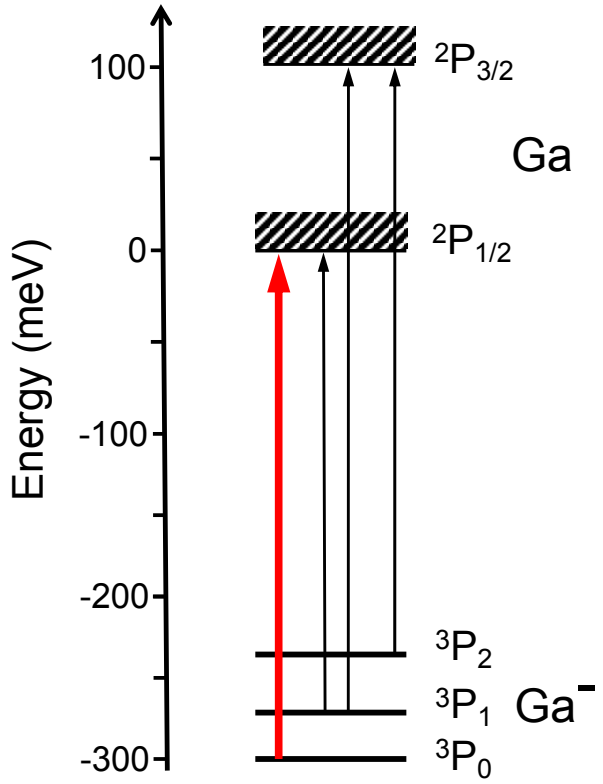

FIGURE 2

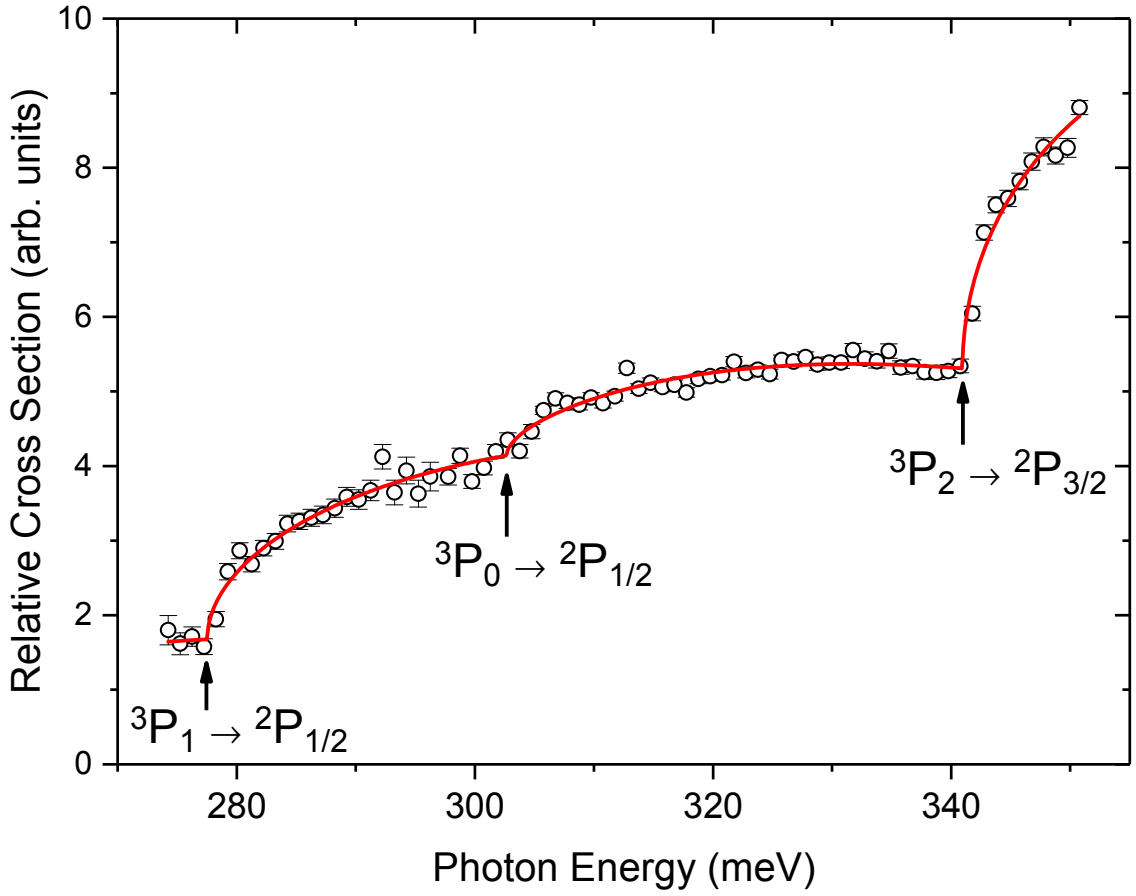
Relative Cross Section (arb. units)
Photon Energy (meV)
0
2
4
6
8
10
280
300
320
340
$^3P_1 \rightarrow {}^2P_{1/2}$
$^3P_0 \rightarrow {}^2P_{1/2}$
$^3P_2 \rightarrow {}^2P_{3/2}$

FIGURE 3

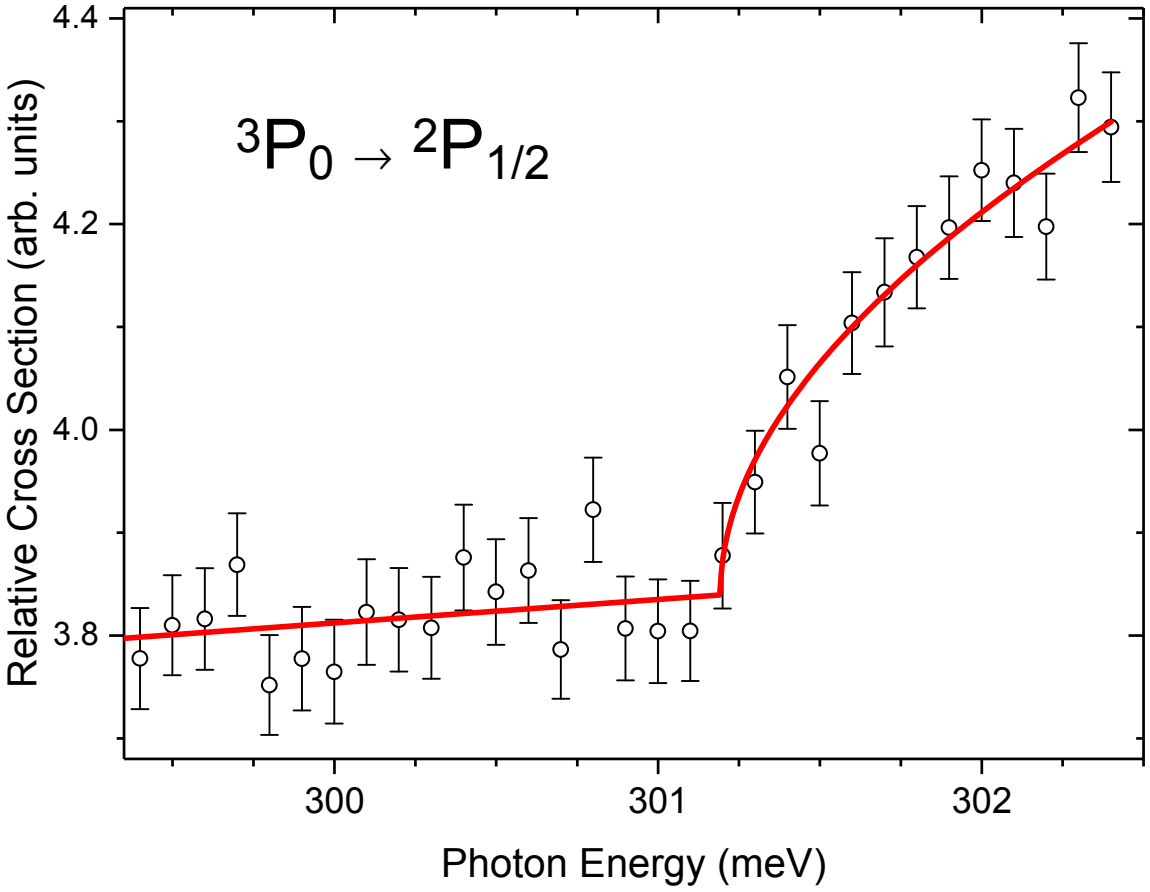
$^3P_0 \rightarrow {}^2P_{1/2}$
Relative Cross Section (arb. units)
4.4
4.2
4.0
3.8
300
301
302
Photon Energy (meV)